Evaluation of the sensitivity of electro-acoustic measurements for process monitoring and control of an atmospheric pressure plasma jet system

V J Law[1], F T O'Neill[2] and D P Dowling[2]

[1]Dublin City University, National Centre of Plasma Science and Technology, Collins Avenue, Glasnevin, Dublin 9, Dublin, Ireland
(e-mail: vic.law@dcu.ie)
2School Mechanical and Materials Engineering, University College Dublin, Belfield, Dublin 4, Ireland

Abstract: The development of non-invasive process diagnostic techniques for the control of atmospheric plasmas is a critical issue for the wider adoption of this technology. This paper evaluates the use of a frequency-domain deconvolution of an electro-acoustic emission as a means to monitor and control the plasma formed using an atmospheric pressure plasma jet (APPJ) system. The air plasma system investigated was formed using a PlasmaTreat™ OpenAir applicator. Change in the electro-acoustic signal with changes in substrate type (ceramic, steel, polymer). APPJ nozzle to substrate distance and substrate feature size were monitored. The decoding of the electro-acoustic emission yields three sub dataset that are described three separate emission mechanisms. The three emissions are associated with: the power supply fundamental drive frequency and its harmonics; the APPJ nozzle longitudinal mode acoustic emission and its odd overtones, and the acoustic surface reflection that is produced by the impedance mismatch between the discharge and the surface. Incorporating this knowledge into a LabVIEW a program facilitated the continuous deconvolution of the electro-acoustic data. This enabled the use of specific frequency band test limits to control the process the APPJ treatment process which is sensitive to both plasma processing conditions and substrate type and features.

PAC Codes: 52.40.Hf, 52.70.-m, 52.77.Fv, 43.60.Vx

Keywords: atmospheric plasma, electrical harmonics, acoustic overtones, surface location, fault detection.

1.0. Introduction

With the increased use of atmospheric plasma systems in applications ranging from polymer surface activation to coating deposition [1, 2] there is a growing need for the development of non-invasive in-situ process monitoring techniques. This paper evaluates the use of electro-acoustic technique as a means of achieving this process monitoring of an atmospheric plasma jet system. Since the late 1990s the acoustic emission from laboratory scale atmospheric pressure plasma jet (APPJ) systems [3, 4], and optical-acoustic studies of plasma welding process [5] have been reported. Following these reports acoustic metrology has been used in the monitoring of anomalous arc discharge in plasma processing equipment plasma [6], plasma and laser welding [7, 8 and 9], and plasma anodizing [10]. More recently plasma acoustic emission metrology has been demonstrated on industrial scale APP reel-to-reel systems [11, 12] and APPJ [13], all of which [11 - 13] have used helium as the working gas.

Experimental observations with physics based interpretation [3, 4, 5 and 6]; time series analysis [7, 8, and 9], neural network analysis [10], and multivariate analysis [11, 12 and 13] have been used to investigate the plasma acoustic emission in an attempt to isolate the specific origin of acoustic emission. In all case it has been observed that the emission signal is complex with parts of the signal associated with specific sources. Eller and Valdivia [14] have developed a multiple frequency approach to identify a generic source. This paper extends this approach to a band of frequencies that have specific origins within the APPJ electro-acoustic emission: these include: drive frequency, jet nozzle flow dynamics and the target process surface. The partitioning of a single observable [15] in to a number of performance parameters that describe the discharge and it surface interaction greatly enhances the metrology measurement and in some cases can provide process information that was not previously available.

The APPJ used in this work is the industrial scale PlasmaTreat Open-Air APPJ manufactured by PlasmaTreat GmbH (Steinhagen, Germany). Amongst the applications of this systems is the manufacture of surface barrier coatings [16] and the activation of polymers [17, 18]. These papers plus [19] give a detailed description of the APPJ. The APPJ is a blown arc [20] that can either use nitrogen or compressed air as the working gas. Spectroscopic studies of these gases, at the nozzle exit, indicate a rotational nitrogen temperature of the order of 3000 - 4000 K for pure nitrogen [19] and 1700 K for compressed air [18]. Thermal and spectroscopic imaging of the discharges has also shown that the discharge flux decreases with discharge axial distance, whilst the thermal diameter has a Gaussian temperature profile which can extend up to 40 mm [18]. Given these gas rotational temperatures and the spatial distribution of the discharge it becomes necessary to control the APPJ nozzle to surface distance and dwell time of the discharge upon the treated surface for temperature sensitive materials.

The objective of this paper is to evaluate the sensitivity of the non-invasive electro-acoustic measurements technique for monitoring and control of the APPJ. In addition to systematically altering the plasma jet processing conditions (plasma cycle time and jet air flow), evaluations carried out were to determine how sensitive the acoustic signal was to changes in substrate type (ceramic, steel, polymer), changes in APPJ nozzle to substrate distance (from 1 to 5 cm) and also substrate feature size.

2.0. Measurement methodology

2.1. The plasma jet system

The plasma treatment studies were carried out using the OpenAir system manufactured by PlasmaTreat GmbH (Steinhagen, Germany). A number of authors have previously described the operation of this APPJ source [16, 17, 18, and 19]. The PlasmaTreat APP jet is driven by a positive dc pulse width modulated (PWM) power source that operates between 19 and 25 kHz and a plasma cycle time (PCT) between 10 and 100%. The PCT value approximates the temporal on-of duty cycle time of the PWM power supply. The APPJ is mounted onto a XYZ gantry which allows the discharge plume to target a 2-dimensional or 3-dimensional process part at parallel speeds up to 30 $m.min^{-1}$. In this work, the parallel speed is fixed rate = 5 $mm.s^{-1}$. A photograph of the APPJ anode-nozzle region illustrates the blown arc protruding from the nozzle as an intense bright-white region, surrounded by a corona-like discharge (figure 2). A schematic of APPJ setup is shown in this figure.

2.2. Non-invasive sensors

Two off-axis non-invasive sensors were used to monitor the APPJ process. These are: an Omni directional condenser microphone (Pro-Signal EM-011), and a sound pressure level meter (YF-20). The two microphones are used to identify microphone related resonances. For comparison a second microphone (Yoga EM070) was tested against the pro-Signal EM-011. For measurements reported here little difference in the APPJ specific electro-acoustic emission was found.

The Omni directional condenser microphone has a 1 kΩ impedance @ 1 kHz, and acoustic frequency range of 1 to 18 kHz. The microphone act as both as a Near-field E-probe and a sound energy sensor, where the measured quantities are distance dependent. The microphone is placed 90 mm from the APPJ nozzle and perpendicular (with a -8 degree off-axis) to the direction of travel. Final the microphone signal passed to the 1 kΩ impedance jack of the computer soundcard.

The sound pressure meter provides a visual reading of the time-average measurement of the APPJ sound level. The measured laboratory back ground sound level for all the measurements reported in

this paper is 60-65 dB. When the APPJ is turned-on, the sound pressure level increased between 90 and 103 dB at an applied dc pulse voltage of 10 kV and PCT values of 10 to 100%.

2.3. Data analysis

The computer used for data collection and processing is a Dell Precision M90 which is fitted with a Sigma Tel Audio soundcard. The data processing software installed is the National Instruments LabVIEW 8.2 software along with the sound and vision tool kit and NI scope. In this configuration electro-acoustic measurement has an unfiltered noise floor = -90 dB/Hz.

The electro-acoustic data is sampled at Nyquist-Shannon criteria [21, 22] sampling rate (S_{ns}) of 120 k $S.s^{-1}$ at a sampling time period (T_p) of 0.1 seconds or 1 second, followed by a Fast Fourier Transform (FFT) to present the data in the frequency-domain at resolution of 1 data point per Hz. Using this sampling protocol (equation 1) the -3 dB bandwidth (B_{-3dB}) equates to 60 kHz.

$$B_{-3dB} = T_p\left(\frac{S_{NS}}{2}\right) \quad (1)$$

A Savitzky-Golay digital filter [23] is chosen to piece-by-piece smooth the data by least square minimisation with a polynomial function ($m = 1$) within a moving window. The windowing is shown in equation 2, where k is the ± sampled data points. For example, using a k value of 10 Hz, this pre-treatment algorithm preserves high frequency components of the power supply drive signal and its harmonics.

$$2k + 1, \quad (2)$$

Finally, three electro-acoustic performance parameters are extracted from the SG filtered data and are used to build process-time history-charts and principal component analysis (PCA) phase-space representation of the APPJ process. These performance parameters or discriptors of the electro-acoustic signal [24] are as follows:

a) A_1: the specific acoustic level (1 Hz) at a given frequency
b) A_2: Averaged specific acoustic emission over a 500 Hz span, at a given frequency
c) A_3: the Mean electro-acoustic emission measured over the total 0-60 kHz span

2.4. Test surfaces

Three treatment surfaces are used in this study. These materials are: a 5 mm thick ceramic base plate,

three stainless steel plates (10 cm in length x 0.2 cm in thickness, and with widths of 1, 2 and 4 cm), and finally temperature sensitive aircraft grade carbon/epoxy weave composite (CWC) (T_g = 150^{o}C) with dimensions of 40 mm x 25 mm x 3 mm. The roughness values of these materials are: Ra = 766 to 1000, 1736 and 790 nm, respectively). The materials are typical of those used in manufacture of sub assembles within the automotive and aerospace industrial [1, 2, and 25]. The use of these test surfaces facilitated the spatial-temporal resolution measurements and evolution of the effect of substrate type on the electro-acoustic signals.

3.0. Results and discussion

The result of the preliminary electro-acoustic analysis data is given in figure 3. This provides a frequency-domain emission comparison between the microphone data and the outcome of the Savitzky-Golay pre-treatment smoothing filter. The acoustic in figure 3 was obtained with a sampling period is 1 second and the APPJ conditions were: PWM drive frequency = 19 kHz, PCT = 50%, compressed air flow = 76.6 l.s^{-1}, and an APPJ nozzle to surface distance = 60 mm. The acoustic sound pressure for this measurement was recorded a 101 dB with a variance of ±1 dB over a time period of 1 second.

The results of the raw un-filtered dataset (gray trace), as shown in figure 3, exhibits a broad continuous amplitude of approximately 25 dB across the frequency spectrum. This broad amplitude response is reflected in the measurement variance of the sound meter. There are also a number of feature present in the data. Firstly the high Q-factor (($f/\Delta f$ -3 dB bandwidth) lines at 19 and 38 kHz are the PWM drive frequency and its second harmonic. The additional line at 8.5 kHz is a sub-harmonic of the PWM process. The other features of note are two broad peaks at 10 kHz and 25 to 30 kHz. Finally the drop in amplitude in the 55 to 60 kHz is associated with the measurement cut-off frequency due to the 120 kHz sample rate of the sound-card.

The second trace (black) in figure 3 shows the result of the SG filtering algorithm. This trace is shown as it is the result of a series of experiments where the windowing was varied to maintain the high frequency of the drive frequency signals. A value of k = 10 Hz produced a filtered noise floor of 100 dB that resulted in a signal-noise-ratio (SNR) of 50 ±3 dB at the 10 kHz peak. This is an improvement of 20 dB in the SRN when compared to the unfiltered signal.

From the examination of figure 3 it becomes self-evident that the microphone acts as a Near-field E-probe due to the fact that the power supply drive frequency and its harmonics are registered above the 18 kHz microphone acoustic range. A further feature of note is that the electrical signals are independent of process conditions [26]. The high value of Q-factor (~200) also implies that the energy loss is low and the loss mechanism is decoupled from discharge. The latter observation is contra to

flyback power supplies and drive circuits that have frequency agile impedance matching [12, 27]. The authors have also noticed that when the APPJ nozzle under goes cleaning maintenance and or when the electrical cabling to the nozzle is upgraded the PWM drive frequency and harmonics can be reduced. These observations highlight that the nozzle electric-field emission is linked to the integrity of the electrical ground return path. Hence the microphone can be used to benchmark maintenance procedures, where any deviation from the prescribed drive frequency signature will indicate an abnormality in the electrical configuration of the APPJ system.

Having established the shape of a typical electro-acoustic scan the focus of this study was to establish the effect on the measured acoustic signals with systematic variation of the parameters detailed in Table 1:

Table 1: Experimental parameters.

Parameter	Value
PWM Drive frequency	19 and 25 kHz
Plasma Cycle time	10-100%
Air flow Rate	37.5 to 76.6 $l.s^{-1}$.
APPJ Nozzle to surface distance	1 to 5 cm
Material: Stainless steel	50 mm x 2 mm x (10, 20 and 40 mm). Mean Ra = 766 nm
Material: Ceramic	50 mm x 2 mm x (10, 20 and 40 mm). Mean Ra 1736 nm
Material: Carbon woven composite	40 mm x 2 mm x 25 mm. Mean Ra 790 nm
APPJ nozzle scan rate	5 $mm.s^{-1}$

The results of this parameter study are detailed in the follow sections: section 3.1, effect of the nozzle to substrate distance: section 3.2, effect of 2D acoustic surface location and: section 3.3 provides a description of surface location as the APPJ is driven in towards the surface from 5 to 1 cm. Section 4 reports on the effect of the surface material (stainless steel, ceramic and carbon woven composite) on the acoustic data.

3.1. Acoustic nozzle analysis- substrate to jet nozzle distance

With the SG filter set at window length of k = ±10 Hz, the electro-acoustic emission was characterised as a function of APPJ to surface distance for a fixed PWM frequency = 19 kHz and PCT = 25 %, and compressed air flow = 76.6 $l.s^{-1}$. The results for 10, 20, 30 and 40 mm gap distance are shown in figure 4. Within this dataset three distinct features are observed. Firstly, the power supply drive at f_o = 19 kHz and its harmonics (f_2 = 28 kHz and f_3 = 57 kHz). These frequencies are constant in frequency position and Q-factor ($f/\Delta f$ -3 dB bandwidth ~200) when the gap position is changed. Second, there is

a broad peak at 10 kHz which has the maximum amplitude of -50 dB and a Q-factor of ~ 10 with a further broad peak at 30 kHz. The third feature of note is the variation in acoustic emission in the 5 to 10 kHz range. In this range the acoustic emission increases as the gap distance is reduced. The sound pressure level measurements also indicates an increase of 1 dB from 101 to 102 dB at a gap distance = 1 cm.

3.1.1 Quarter wave-length model

The second feature identified in figure 4 is the broad peak (Q-factor ~10) at 10-11 kHz. It is modelled mathematically using the closed air-column (clarinet) approached described by Law et al [13]. The approach used here is to employ the quarter standing-wave phenomenological equation 2 to describe the longitudinal mode within the discharge. The azimuthal and radial modes are not considered here as their frequencies are above the 50 kHz range. In equation 3, n is modulo frequency number, L is the physical length of the nozzle (L = 8 mm), 0.6r is the end correction [28], where r is the internal radius of the nozzle) and c_{sound} is the sound velocity in air. For this quarter wave model the exit aperture of the nozzle defines the maximum pressure vibration, and the internal nozzle aperture, where the compressed air (1.5 atmospheres) enters, is the antinode. Using this configuration only the fundamental and odd number overtones are supported. For example, f_o and n = 3, 5, etc…

$$f_n = \frac{nc}{4(L + 0.6r)} \tag{3}$$

At room temperature (25^{o}C) the speed of sound in air equates to 346.26 m.s^{-1}, using this sonic value, equation 3 yields frequency values of f_n = 9.11 kHz, f_3 = 27.33 kHz, and f_5 = 45.55 kHz. The values of f_n and f_3 = 3 approximates to the broad peaks in figure 3 and figure 4.

To provide further supporting evident of the quarter-wavelength model, the time-domain APPJ acoustic envelope (as captured by the microphone) is shown in figure 5. This measurement clearly shows a square waveform with a 50% duty cycle and a mean frequency of the order of 10 kHz. From a mathematical point of view, harmonic deconstruction of this waveform requires a Sinewave of the fundamental and series of odd numbered integer overtones (harmonics) of the fundamental Sinewave. The time-domain acoustic envelope also reveals similar rise (attack) time and fall (release) time of 0.1 milliseconds, and a sustained time period of 1 millisecond. In addition, with the sustained period the PWM drive frequency can be observed. These results confirm that the PWM frequency is being pulse modulated by the acoustic production of the APPJ nozzle.

3.1.2 Helmholtz resonator

Rat and Cloudert et al [20] have proposed that the nozzle acoustic can be modelled as a *Helmholtz*

resonator. In our paper we explore this idea by evaluating the APPJ nozzle using equation 4. In this equation the volume of air in the cathode cavity (V_o) has a spring constant that is inversely proportional to its volume (V_o). The nozzle length (L) appears in the denominator because of the inertia of the air in the nozzle is proportional length. The cross-section area (A) has a two fold effect; 1) as the area increases the air velocity decreases; and 2), the inertia of the air decreases with A.

$$f_n = \frac{C_{sound}}{2\pi}\sqrt{\frac{A}{LV_o}} \tag{4}$$

Using a cavity volume of 1 x10^{-5} cm^3 and a cross-sectional area of 19.6 x10^{-5} m^2, equation 4 yields an acoustic frequency of the order of f_n = 2.7 kHz. This value is 4 times smaller than the computed value in equation 3: to match computed values of equation 1, V_o would have to be 12 times smaller. When the operating pressure conditions of the APPJ are considered (the cathode cavity pressure ~ 1.5 atmospheres, and an exit nozzle pressure ~1 atmosphere) it appears that the springiness of the air has been lost. This implies for the *Helmholtz resonator* model to work, V_o must be reduced to small fraction which surrounds the internal nozzle entrance. A further feature to be taken into consideration is that there is no modulo component to predict the odd numbered overtones.

Equation 3 and 4 enable partial de-convolution of the nozzle emission from the APPJ electro-acoustic signal. A simple comparison between these equations suggests that the clarinet quarter-wave model (equation 3) may present the most realistic representation of the acoustic fundamental frequencies and the overtones of the nozzle.

A further set of measurement were performed to examine the effect of air gas flow. Figure 6 presents the results for 37.5 (black solid line) and 76.6 l/s (dotted gray line) for the following plasma conditions; PWM = 19 kHz, PCT = 100% and a nozzle to surface distance of 1 cm. The results demonstrate that the main peak feature observed in figure 4 is also recorded here in figure 5. However there are a number signal feature that are different. For example the 37.5 $l.s^{-1}$ trace exhibits a dip in amplitude in the 20 to 25 kHz range and there is also present a series of quasi periodic (2 kHz) features emanating from the nozzle signature at 10 kHz. In comparison the high air flow (76.6 $l.s^{-1}$) trace has no amplitude dip in the 20 to 25 kHz range, and also the general amplitude is enhanced by approximately 6 dB from 20 kHz. The low air flow measurement is in-line with the quarter-wavelength nozzle analysis, in the nozzle signature (10 kHz) and the 3rd overtone (30 kHz) is observed. The overall increase in signal amplitude for the high air flow is also consistence with expected increase in air pressure around the measurement zone.

3.2. Vertical surface location

In this section the electro-acoustic emission is measured as the APPJ is driven into the treated surface, and the electro-acoustic performance parameters: A1 (at 8 kHz), and A_3: (0 to 60 kHz) are used to locate and define the surface as a function of nozzle to surface distance. The data is collected using a sampling period of 1 second with sample resolution of 1 Hz within the 0-60 kHz frequency span. The surface location measurement is performed by reducing the nozzle-to-ceramic surface gap distance.

Consider first the frequency band that is most strongly associated with the surface. The topology of this frequency band is markedly different when compared to the electrical signal of the power supply and the acoustic nozzle signature: that is the surface signature is flat and broad. Given this contrasting difference, the APPJ appears to act as a compact sound source (5 mm nozzle aperture) above the flat reflecting surface with the reflected pressure having a spherically radiated distribution that is not only symmetric around the discharge impact epicenter, but also reflects from the whole of discharge flux at the ceramic surface which can be up to 40 mm in diameter. Under these reduced gaps distance conditions the microphone becomes aligned to the treated surface level and where a steady increasing proportion the discharge gas flow will be deflected into the microphone location with varying phase delays with respect to the sonic pressure wave arriving directly from the nozzle. A simple comparison between these two pressure waves (S_{ound} = 346.26 m.s^{-1}) and reflected particle velocity pressure wave (1.28 m^3.s^{-1} divided by area of nozzle (1.96 x 10^{-5} m^2) = 65 m.s^{-1}) indicates the reflected pressure wave takes approximately 5 times as long to reach the microphone. The signals derived from the drive frequency (and nozzle) will be primarily acoustic in nature, whereas the surface signal will be driven by the reflected gas pressure: and hence will have a broad frequency component due to large reflection zone of the discharge at the treated surface.

A typical example for a specific acoustic level (A_1 = 8 kHz) developed at the microphone as the nozzle to surface distance is reduced from 50 to 10 mm is shown in figure 7. In this figure the discharge is turned on at t = 3s with the nozzle gap set at 50 mm. At t = 15s the nozzle gap distance is reduced to 10 mm. At this point the A_1 measurement increases by approximately 5 dB. At t = 34s the plasma is turned-off and where the signal returns close its original acoustic amplitude.

Returning to the A_3 measurement, this value is plotted in figure 7 for the same process conditions. This measurement follows the process temporal evolution of the A_1 signal although at a reduced magnitude (2-3 dB at t = 15s). This additional acoustic parameter adds additional robustness to the identification of the inflection point.

A further set of microphone fixed off-axis position experiments indicate that changing the microphone position by a centimetre in either the XYZ direction does not significantly change the acoustic peaks

frequencies and that the acoustic performance parameters, A_1 and A_2 could still be used. This observation is similar to the change in amplitude and bandwidth as reported for acoustic monitoring of plasma welding processes [6].

3.3. PCA of vertical acoustic surface location

In the previous section two performance parameters were deconvolved from a single observable, namely the electro-acoustic signal, and used to construct a process time chart of the APPJ-ceramic interaction. In order to employ principal component analysis (PCA), in terms of a loading plot, it is necessary to introduce an additional performance parameter. The advantage of using 2D PCA loading plot is that the constructed phase-space provides higher-dimensional coordinate systems where the heterogeneous plasma-surface process is directly mapped. Within this coordinate system the process is tracked and visualized in real-time with clusters of data points representing different process states for atmospheric plasma [11, 12, and 13] and low pressure plasma [28]. For example: start, nozzle-surface gap distance, and finish. Moreover, the vector data points between the clusters represented the process transition between the state clusters.

Figure 8 shows the results of this 2D mapping procedure for the APPJ-ceramic process as described in section 3.2. At the bottom left of figure 8 the cluster is associated with the discharge turned-off condition (the start and the finish of the APPJ process). The centre of mass of this cluster is: A_3 = -102 dB and A_1 = -90 dB. As the discharge is tuned on a new XYZ cluster centre of mass coordinate is formed (A_3 = -63 dB and A_1 = -58 dB) that is associated with the APPJ nozzle positioned at 5 cm over the ceramic surface. A third cluster is formed (A_3 = -63 dB and A_1 = -55 dB) as the APPJ nozzle gap distance is reduced to 1 cm. In terms of A_1, This third cluster is +5 dB above the second cluster. The sampling data sequence provides a time evolving picture of the APPJ-ceramic process with the advantage that fault prediction capability is introduced into the map. For example, when the x and y score values fall outside of predetermined range a new cluster state is formed and a deterministic fault condition has occurred [29].

In order to estimate the gap distance sensitivity of the 2D mapping process, non-parametric cluster analysis [11] is employed to judge the separation between clusters. Here each cluster area is evaluated in Cartesian space and the spacing between each cluster is measured in terms of the area the cluster. For example, the start/finish state cluster has a area of A_3 = 1 dB x A_1 = 6 dB, and the separation from the 5 and 1 cm state clusters is of the order of 20 A_1 units. The separation between the 5 and 1 cm state clusters however is very much reduced. However when viewed as a A_1 score histogram (figure 8 insert) the 5 cm cluster data reveals a Gaussian distribution with a mean = - 70 dB and the 1 cm cluster data has a positive Skewnegess with a mean = -65.5 dB indicating a surface deterministic effect. Using this cluster analysis an estimation of the gap distance is of the order of 1 dB per 1 cm.

4. Scanning acoustic macroscopy

The objective of this study is to determine the ability of the acoustic signal to detect different materials as the APPJ scans across a treatment surface (for example, the activation of sub assembly headlight fixtures before bonding) it is necessary to consider the spatial resolution of the acoustic measurement. In this study the scanning of the APPJ over alumina ceramic flat surface onto which has a steel strip with dimensions 40 mm wide x 10 cm in length and 2 mm thick is placed. In order to capture one data point per mm along the width of the steel 40 data points per scan is required. For an APPJ scan rate = 5 $mm.s^{-1}$, the sampling period needs to be of the order 0.1 second. This calculation assumes that the APPJ discharge flux area is of the order of 1 mm in diameter. In practice, the discharge flux area varies from approximately 1 cm at the nozzle to 4 cm in diameter at an axial afterglow distance of a few centimetres [18]. Additional factors that will influence the spatial resolution include the surface roughness Ra value, the surface patterning, and height difference. These spatial and material factors are examined in the following four experimental measurements (figures 9, 10, 11, and 12).

Figure 9 shows the A_2 performance parameter (500 Hz, at 8 kHz) as the APPJ is scanned at a rate = 0.5 $mm.s^{-1}$over the ceramic base with a stainless steel plate as a function of nozzle to base distance 1, 1.5, 2.0, 2.5 and 3 cm above the ceramic base. The steel width is 4 cm. The plasma condition used here are PWM = 25 kHz, PCT = 50%, and 76.6 $l.s^{-1}$ of compressed air. The data sampling period = 0.1 seconds.

The 1 cm trace measurement reveals a clear response to the steel plate as seen by the negative amplitude (1 to 2 dB) discontinuities at $t \sim 2.5$ seconds and $t \sim 7$ seconds. The difference in the first and second steel edge profile is due to 8 degree miss-alignment of the microphone position as determined by microphone reposition follow-up measurements.

The remaining traces (1.5 to 3 cm) shows that as the gap distance is increased the steel edge registrations are reduced in amplitude. Note for the 3 cm trace the edge registration is reduced in to the over-all noise level with respect ceramic and steel surface regions. At this nozzle to surface distance where the relatively cool (300 K [18]) afterglow of the discharge is impinging on the materials. Time-series analysis in the form of windowed standard deviation and variance calculations are required to extract the surface location information. For example at the time values regions of t = 0.5 and 4.5 seconds, amplitude variance (maximum to-minimum) is of the order of 0.8 dB. Whereas in the initial edge scatting region (t = 2 to 3 seconds) the amplitude variance is approximately 2 dB. This change in variance as the discharge flux traverses the ceramic and steel surface allows the surface detection and location measurement to be extended further into discharge.

The temporal profile of the edge signatures and the time distance between them enables an estimation of the spatial resolution of the measurement. For example, the time difference between the discontinuities is approximate 4.5 seconds, and the scam rate is 5 $mm.^{-1}$: these values yield a steel width of 2.1 cm. Additionally the time span of the edge discontinuity are approximately 1 cm, which equates to 0.5 cm. trace has a typical edge profile time of 1 second, and using the knowledge that the scan rate = 5 $mm.s^{-1}$, this equates to a observable linear surface distance of 0.1 cm.

In terms of discharge chemistry it can be stated that the 1 cm time-trace is closely associated with the blown arc region where the nitrogen gas rotational temperature in air discharge is of the order of 1700 K [18]. For the 1.5 to 3 cm trace the afterglow chemistry impinging at the surface becomes progressively dominated by the cooler (300K) recombination process of $N + NO \rightarrow NO_2^*$ chemistry. At present it is unclear how the chemistry affects the acoustic signal. This aspect of the measurement needs further investigation. However from the above measurements, it is reasonable to assume that the edge discontinuities are most likely to the results of acoustic scattering as the discharge flux transits these regions.

To gauge whether the plasma cycle time (PCT) parameter which is expressed as a percentage has an effect on the surface location measurement a series of measurements were performed with varying values of PCT% and a fixed nozzle to surface distance. Figure 10 provides an example of surface location at a nozzle to surface distance of 1.6 cm as a function of fixed PCT percentages (10, 20, 40, 60, 80 and 100%) at a PWM frequency = 25 kHz. Each measurement was made individually and for comparison purposes the traces are then aligned second steel edge profile at $t \sim 7.5$ seconds. Here again the difference in the first and second steel edge is due to 8 degree miss-alignment of the microphone position. From these series measurement it is concluded that varying the PCT percentage at the fixed PWM frequency = 25 kHz has very little affect on the electro-acoustic data.

4.2 Scanning across different materials.

In this section the acoustic response to different substrate materials e.g., stainless steel, ceramic and composite) are examined.

Figure 11 depicts the acoustic response of three different widths of (1, 2, and 4 cm) stainless steel (Ra = 766 nm) on a ceramic base (Ra =1736 nm) at a nozzle to surface distance = 1 cm. The discharge conditions: PWM = 25 KHz, PCT = 50%. The measurements reveal that all three widths of the steel can be resolved, even though the microphone remains off-centre by 8 degrees. The striking feature of this comparison that the 1 cm sample allows a estimation of the degree in which the edge signal extends in to the physical dimension of the steel plate. For example, given a steel width (1 cm) and a

scan rate (5 $mm.^{-1}$) the physical width of the steel equates to 2 seconds on the graph. This indicate that the edge profile response extend approximately 2 mm over the steel surface. The acoustic response of the 2 and 4 cm wide steel plates are inline with is observation indicating the robustness of the measurement. It is also worth noting that the greater microscopic roughens of the ceramic does not appear to affect the acoustic response of the two materials.

Figure 12 depicts the acoustic response of stainless steel on a steel base for the three different width of steel (1, 2, and 4 cm) at a nozzle-to-base distance = 1 cm. discharge conditions: PWM = 25 KHz, PCT = 50%. These measurements are similar to those depicted in figure 9 indicating that the edge effect is present when the base material is the same as the treated metal. In this series of measurement the microscopic roughness of the two materials is the same. From this it can be concluded that edge profiles have a greater effect on the signal rather than the microscope roughness of the materials.

Figure 13 depicts the acoustic response of 2.5 cm wide and 3 mm thick aerospace grade carbon/epoxy weave composite (CWC) on a stainless steel (Ra = 766 nm) base, a ceramic (Ra = 1736 nm), and CWC (Ra = 790 nm). The nozzle-to-base surface distance = 1 cm, with discharge conditions: PWM = 25 kHz, PCT 50%. The results of this series of measurement show that the CWC gives a strong response and that the physical width can be resolved. The comparison between the base materials also shows that the CWC on CWC trace produces the greatest response in terms of edge profile and surface amplitude response. Here again the Ra value does not appear to play a dominate in the acoustic response. To further examine the edge effect additional differential surface height measurements were made. The outcome of these measurements indicated that the reduced nozzle distance influences the acoustic signal rather than the microscopic surface roughness. The influence of weave pattern within the CWC upon the acoustic response is still understood and requires further investigation.

5.0. Process control using hard and soft limits

Sections 3 and 4 have examined the electro-acoustic frequency domain response of the APPJ system under varying process parameters. The information obtained from these studies allows the electro-acoustic single observable to tested for specific conditions at discrete frequency bands. For the APPJ system studied here, the frequency bands are associated with the surface, nozzle and PWM drive frequency and it harmonics. This procedure can be readily implemented in LabVIEW software using lower and upper limits at the discrete frequency bands. When the signal amplitude breaches these limits, an out of bound condition fail is registered and a simple audio-visual alarm is triggered to warn the operator of the. A binary code (0 or 1) from the comparator [29] may also be hard wired to the APPJ system for data logging. Depending upon the nature of the out of bound condition, the binary code may also be used to shut down the plasma process. Figure 14 depicts the LabVIEW software

front panel display of the electro-acoustic single observable for a ceramic surface. In this PWM = 19 kHz example, the signal has breached the 4 to 8 kHz surface limit frequency band that has been set to an amplitude of -55 dB. Note here that the PWM drive frequency and its harmonics ($f_{n=2}$ = 38 kHz, and $f_{n=3}$ = 57 kHz)) are not breached. It is clear from the composite on composite (figure 13) that the surface limit would have to be increased in order for the gap distance data to pass the process settings.

6.0. Conclusion

In this study the sensitivity of the electro-acoustic signals to change in PlasmaTreat atmospheric pressure plasma jet processing conditions and substrate /feature size are evaluated. The partitioning of atmospheric pressure plasma generated electro-acoustic emission (single observable) into three sub datasets has been successfully demonstrated. The decoding of this single observable allow discrete frequency bands to be monitored for a specific state condition (power supply, jet nozzle, and surface reflection). This knowledge forms the basis of an automated APPJ control algorithm. The data for the APPJ control algorithm is collected from an off-axis condenser microphone that acts as a Near-field E-probe.

The Near-field electric information enables the discharge drive frequency and it harmonic (f_o plus $f_{n=2\ to\ 5}$) to be identified and monitored for performance. The advantage of this measurement, are three fold: 1, evaluation of the correct drive frequency has be selected, 2, run-to run fault monitoring and 3, post maintenance certification of the cleaning and reassembly of the APPJ nozzle.

The condenser microphone also provides information on the APPJ nozzle acoustic performance. In this paper, both quarter-wavelength air column model and the *Helmholtz resonator* model have been tested against the nozzle signature. In terms of f_n and odd overtone $f_{n=3\ and\ n=\ 5}$, the quarter wavelength model was found to provide the best nozzle description. Time-domain measurement of the acoustic signature provide additional supportive evident the quarter-wavelength model.

It has been established that the signal associated with the APPJ surface interaction is broadband in nature and has no harmonic content (as compared to the electrical and sonic nozzle data subsets). It is likely that this broadband characteristic arises from the discharge flux gas being scattered from the treatment surface, part of which is directed into microphone head. Using this assumption process-time time-history charts can be used to monitor the plasma process. PCA analysis in the form of a 2D phase-space plot may also be used to follow the discharge-surface interaction, both as a function static height (with a sensitivity of 1 dB per cm in the range of 1 to 5 cm), and in the scanning acoustic macroscopy mode with a spatial-temporal resolution of the order of 0.1 cm over steel, ceramic and carbon/epoxy weave composites. The surface resolution (sensitivity) may be ranked as follows: height>edge dimension>material type. With the addition of a data variance algorithm the

measurement can be extended to the down-stream region of the discharge where temperature sensitive materials are processed. Finally, this knowledge of nozzle to surface distance is of particular importance for temperature sensitive materials as the discharge temperature decays with discharge axial distance.

Acknowledgements

This work is supported by Science foundation Ireland 08/SRC/I1411.

6.0. References

[1] Suchentrunk. R, Fuesser. H. J, Staudigl. G, Jonke. D, and Meyer. M. Plasma surface engineering - innovative processes and coating systems for high-quality products. Surface and Coatings Technology. 112, (1-3)351-357. 1999.

[2] Kim J. K, Kim H. S, and Lee. D. G. Adhesion characteristics of carbon/epoxy composites treated with low- and atmospheric pressure plasmas. J Adhesion Sci. Technol. 17(13) 1751-1771, 2003

[3] NakaneT,, Miyajima. T, and Otsuka. T. Current waveforms of electric discharge in air under high-intensity acoustic standing wave field. Japn. J. Appl. Phys. 43(5B), 2852-2856, 2004.

[4] Pekárek. S, and Bálek. R. Ultrasound and airflow induced thermal instability suppression of dc corona discharge: an experimental study. PSST. 15, 52-58, 2006.

[5] Farsona. D. F, and Kim. K. R. Generation of optical and acoustic emissions in laser weld plumes. J Appl Phys. 85(3), 1329-1336, 1999.

[6] Yasaka. M, Takeshita. M, Miyagawa. R. Detection of supersonic waves emitted from anomalous arc discharge in plasma processing equipment. Japn. J. Appl. Phys. 39, L1268-L1288, 2000.

[7] Wang. Y, and Zhao. P. Noncontact acoustic analysis monitoring of plasma arc welding. Pressure vessels and piping. 78, 43-47, 2001.

[8] Szymanski. S, Hoffman. J, and Kurzyna. J. Plasma plume oscillations during welding of thin metal sheets with a Co_2 laser. J Phys. D: Appl, Phys. 34 189-199, 2001.

[9] Saad. E, Wang. H, and Kovacevic. R. Classification of molten pool modes in variable polarity plasma arc welding based on acoustic signature. J. Mater. Proc. Technol. 174, 127-136, 2006.

[10] Boinet. M, Verdier. S, Maximovitch. S, Dalard. F. Application of acoustic emission technique for in situ study of plasma anodizing. NDT&E International. 37, 213-219, 2004.

[11] Law. V. J, Tynan. J, Byrne. G, Dowling. D. P, and Daniels. S. The application of multivariate analysis tools for non-invasive performance analysis of atmospheric pressure plasma. Chaotic Systems: Theory and Applications. 147-154, Ed by C. H. Skiadas and I. Dimotikalis. (World Scientific Publishing 2010). ISBN 978-981-4299-71-8.

[12] Tynan. J, Law V. J, Ward. P, Hynes. A. M, Cullen. J, Byrne. G, Dowling. D. P, and S. Daniels. S.. Comparison of pilot and industrial scale atmospheric pressure glow

discharge systems including a novel electro-acoustic technique for process monitoring, PSST, **19**, 015015, 2010.

[13] Law. V. J, Nwankire. C. E, Dowling. D. P, and Daniels. S. Acoustic emission within an atmospheric helium corona discharge jet. CHAOS2010: 3rd Chaotic modeling & simulation international conference. Chania, Crete, Greece. 1-4th June 2010. Abstract published by the organizing Committee within the CHAOS2010 book of abstracts, pp44, and http://cmsim.net/id16.html

[14] Eller. M, and Valdivia. N. P. Acoustic source identification using multiple frequency information. Inverse Problems 25, 115005, 2009.

[15] Walsh. J L, Iza. F, Janson. N. B, Law. V. J, and Kong. M. G. Three distinct modes in a cold atmospheric pressure plasma jet. J, Phys, D: Appl, Phys **43**(7), 075201 (14pp), 2010.

[16] Scopece. P, Viaro. A, Sulcis. R, Kulyk. I, Patelli. A, and Guglielmi. M, SiOx based gas barrier coatings for polymer substrates by atmospheric pressure plasma jet deposition, Plasma Process. Polym. **6**(S1), S705-S710, 2009.

[17] Lommatzsch. U, Pasedag. D, Baalmann. A, Ellinghorst. G, and Wagner, Hans-Erich. Atmospheric pressure plasma jet treatment of polyethylene surfaces for adhesion improvement, Plasma Process. Polym. **4**(S1), S1041–S1045, 2007.

[18] Dowling. D. P, O'Neill. F. T, Langlais. S. J, and Law. V. J. Influence of dc pulsed atmospheric pressure plasma jet processing conditions on polymer activation. Submitted to Plasma Process Polym. September 2010.

[19] Kubota. Y, Ichiki. R, Hara. T, Yamaguchi. N, and Takemura. Y. Spectroscopic analysis of nitrogen atmospheric plasma jet. J. Plasma Fusion Res. 18, 740-743, 2009.

[20] Rat. V, Coudert. J-F, Denoirjean. A, and Montavon. G. Blown arc plasma source for the elaboration of finely structured coatings. The Open Plasma Physics Journal. 2, 133-149, 2009.

[21] Nyquist. N. Certain topics in telegraph transmission theory. Trans AIEE. **47,** 617-644, 1928

[22] Shannon. S. E,. Communication in the presence of noise. Proc. Institute of Radio Engineers. **37**(1), 10-21, 1949.

[23] Savitzky. A, and Golay. M. J. Smoothing and differentiation of data by simplified least squared procedures. Analitical chemistry **36**(8), 1627-2639. 1964.

[24] Zdunek. A, Konopacka. D, and Jesionkowska.K. Crispness and crunchiness judgment of apples based on contact acoustic emission. Journal of Texture Studies. **41** 75–91,

2010.

[25] Ramamurthy. A, Mohan.J, Murphy. N, Ivankovic. A, and Dowling. D. P. Enhanced carbon/epoxy composite fracture toughness achieved using atmospheric pressure plasma. Adhesion Society, Florida, Feb. 2010

[26] Law V. J, Daniels. S, and D. P. Dowling. D. P.. A generalized electro-acoustic model for laboratory and industrial scale atmospheric pressure plasma jets. GEC2010 (LW2 plasma jets) Paris, France.

[27] Nwankire. C. E, Law. V. J, Nindrayog. A, Twomey. B, Niemi. K, Milosavljević. V, Graham. W. G, and Dowling. D. P. Electrical, thermal and optical diagnostics of an atmospheric plasma jet system. Plasma Chem, polym, processing. **30**(5) 537-552, 2010.

[28] Levine H, and Schwinger. J. On the radiation of sound from an unflanged circular pipe. Physical Review. **73**(4) 383-406, 1948.

[29] Law. V J, Macgearailt. N. Visualization of a dual frequency plasma etch process. Meas, Sci, Technol. **18**(3), 645-649, 2007.

Figure Captions

Figure 1: Photograph of APPJ discharge

Figure 2: Side and top view schematics of APPJ and off-axis sensors.

Figure 3: Comparison between raw and SG (k = ±10) filtered frequency domain data.

Figure 4: Savitzky-Golay filtered APPJ electro-acoustic emission as a function of fixed gap distance at an air flow rate = 76.6 $l.s^{-1}$.

Figure 5: Time-domain acoustic envelope measurement of APPJ acoustic emission.

Figure 6: Savitzky-Golay filtered APPJ electro-acoustic emission as a function of air flow, at a fixed nozzle to surface distance of 10 mm.

Figure 7: A_2 (6 kHz) and A_3 (0 - 60 kHz) time-history chart as function of process time and nozzle gap distance.

Figure 8: 2-D phase-space representation of non-scanning APPJ-ceramic surface process.

Figure 9: A_2 and gap distance = 1, 1.5, 2, 2.5 and 3 cm. Scan rate = 5 $mm.s^{-1}$. For clarity the traces are offset by 50% from the 1 cm trace.

Figure 10: A_2 PCT dependency (10, 20, 40, 60, 80 and 100%). Discharge conditions: 25 kHz, PCT = 50%, gap distance 1 cm. Scan rate = 5 $mm.s^{-1}$. For clarity the additional traces have been give a positive offset from the PCT = 10% trace.

Figure 11: A_2 spatial resolution measurement as function fixed width (1 cm, 2, cm and 4 cm) for steel on ceramic. Discharge conditions: 25 kHz, PCT = 50%, gap distance 1 cm. Scan rate = 5 $mm.s^{-1}$.

Figure 12: A_2 spatial resolution measurement as function fixed width (1 cm, 2, cm and 4 cm) for steel on steel. Discharge conditions: 25 kHz, PCT = 50%, gap distance 1 cm. Scan rate = 5 $mm.s^{-1}$.

Figure 13: A_2 spatial resolution measurement for composite on x (x = steel, ceramic, or composite). Discharge conditions: 25 kHz, PCT = 50%, gap distance 1 cm. Scan rate = 5 $mm.s^{-1}$.

Figure 14: LabVIEW screen data demonstrating how the system can be used for process control. In this case ‘Fail’ is associated with in the 4 to 8 kHz frequency range.

Figure 1

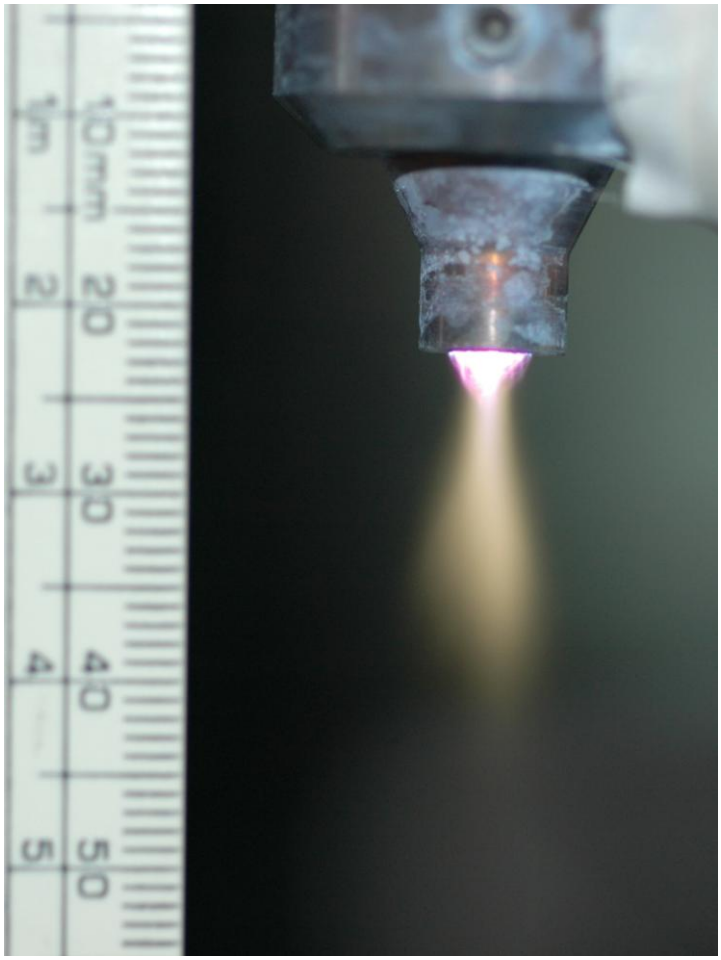

Figure 2

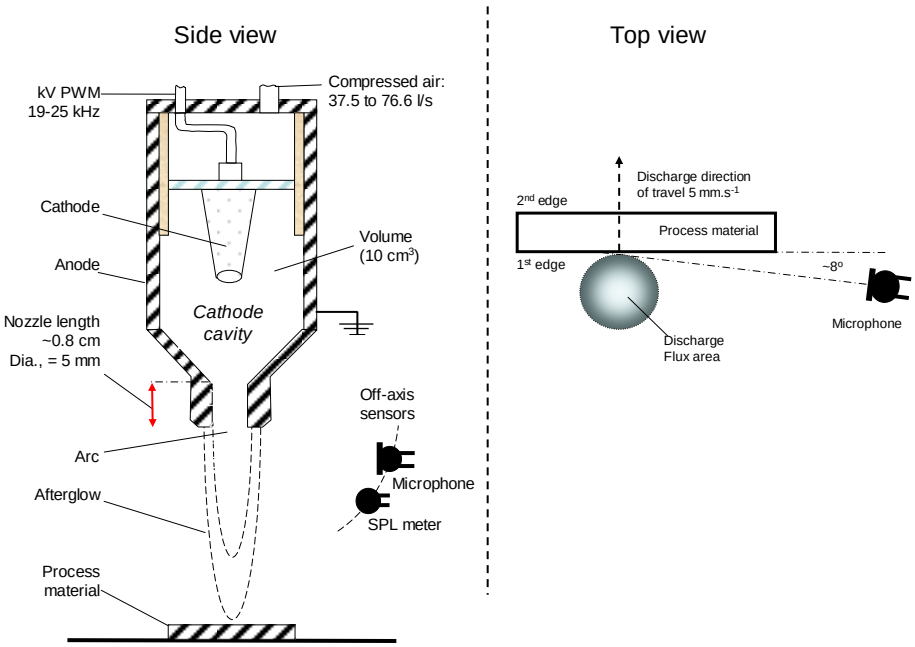
Side view
Top view
kV PWM
19-25 kHz
Compressed air:
37.5 to 76.6 l/s
Cathode
Anode
Volume
(10 cm3)
Cathode
cavity
Nozzle length
~0.8 cm
Dia., = 5 mm
Arc
Afterglow
Process
material
Off-axis
sensors
Microphone
SPL meter
Discharge direction
of travel 5 mm.s-1
2nd edge
Process material
1st edge
~8°
Microphone
Discharge
Flux area

Figure 3

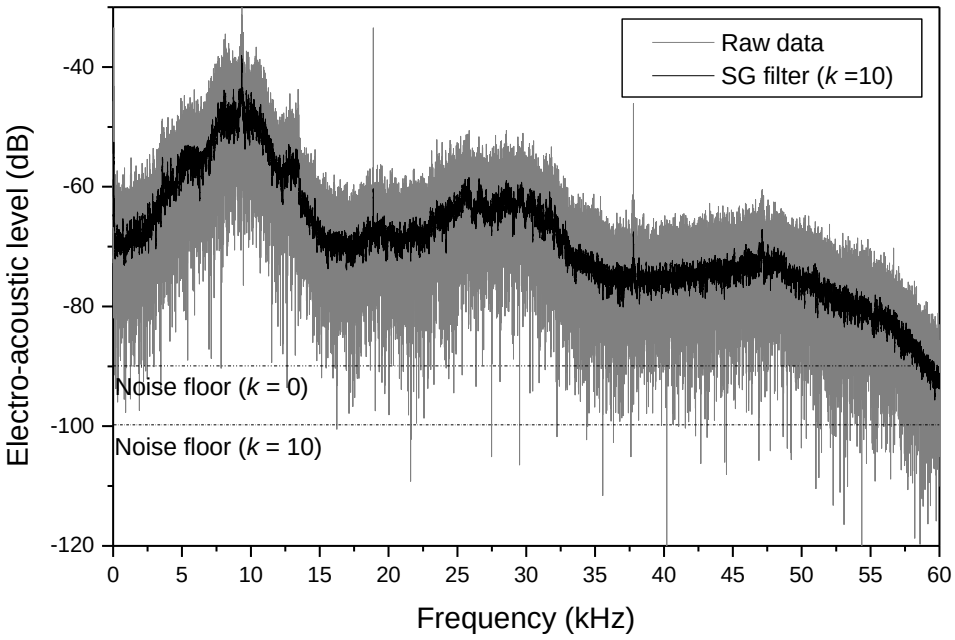
Raw data
SG filter (k =10)
Noise floor (k = 0)
Noise floor (k = 10)
Electro-acoustic level (dB)
-40
-60
-80
-100
-120
0
5
10
15
20
25
30
35
40
45
50
55
60
Frequency (kHz)

Figure 4

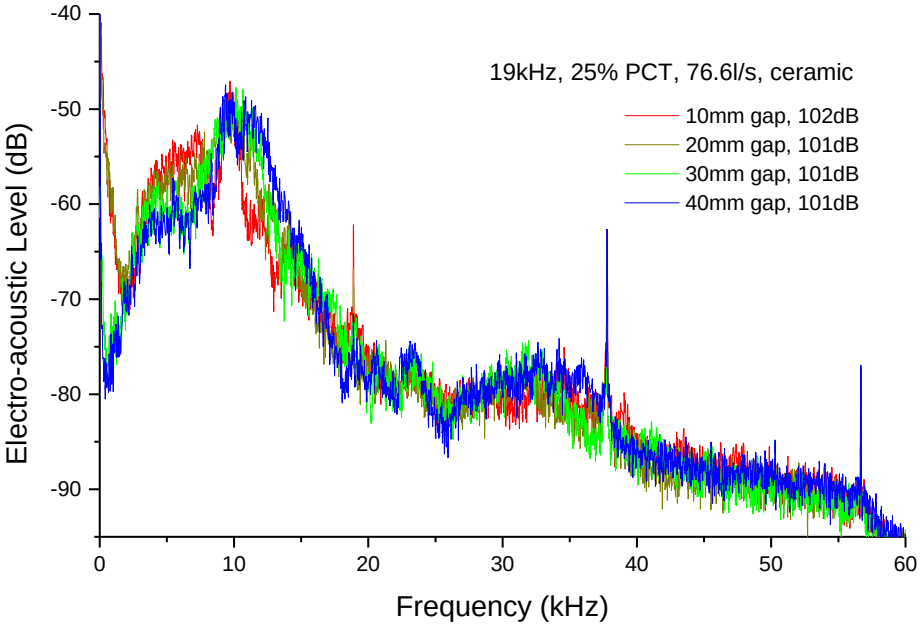
19kHz, 25% PCT, 76.6l/s, ceramic
10mm gap, 102dB
20mm gap, 101dB
30mm gap, 101dB
40mm gap, 101dB
Electro-acoustic Level (dB)
-40
-50
-60
-70
-80
-90
0
10
20
30
40
50
60
Frequency (kHz)

Figure 5

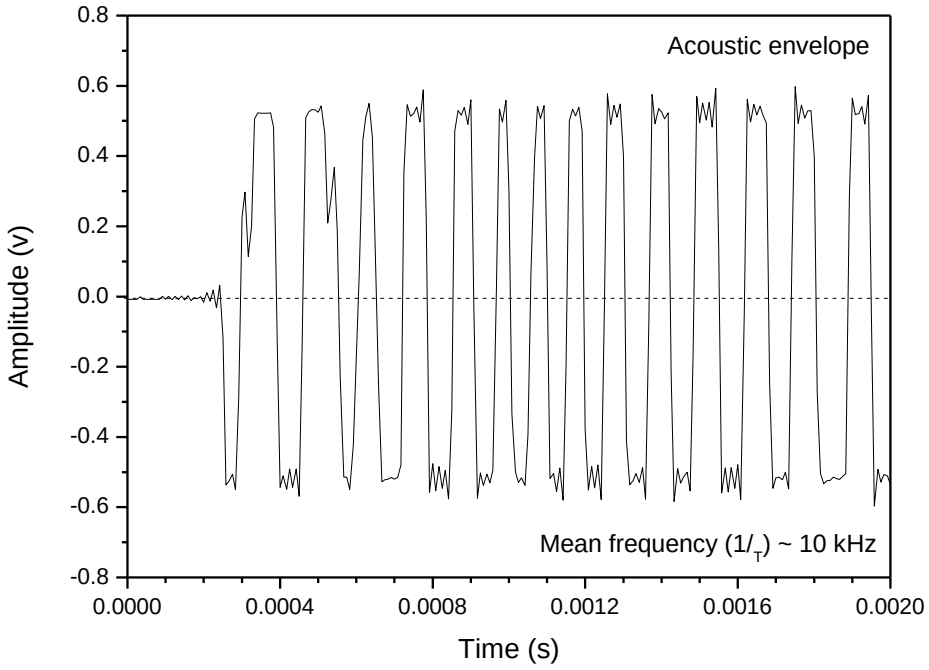
Acoustic envelope
Mean frequency (1/T) ~ 10 kHz
Amplitude (v)
Time (s)
0.8
0.6
0.4
0.2
0.0
-0.2
-0.4
-0.6
-0.8
0.0000
0.0004
0.0008
0.0012
0.0016
0.0020

Figure 6

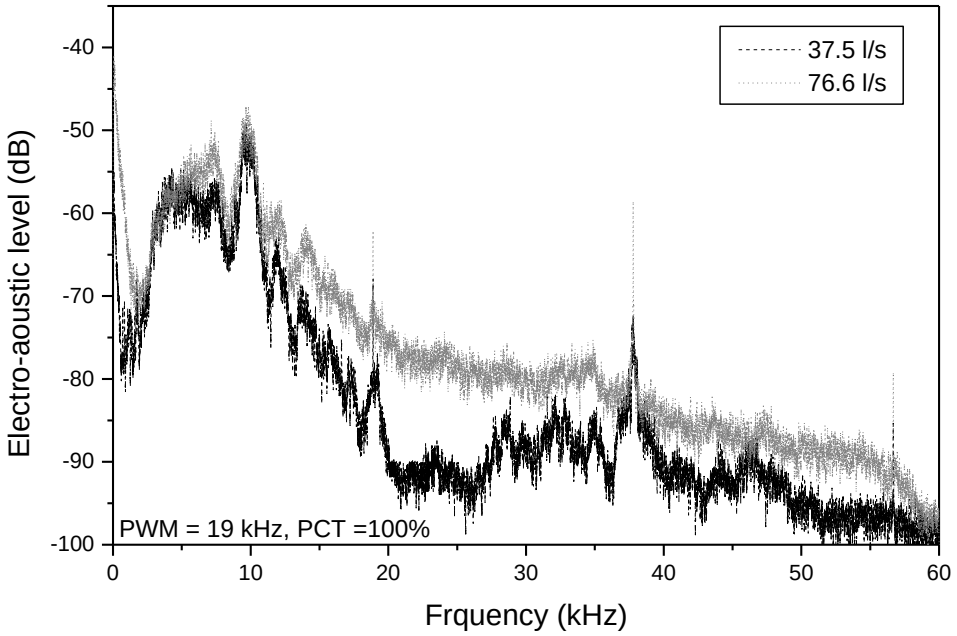
37.5 l/s
76.6 l/s
Electro-aoustic level (dB)
-40
-50
-60
-70
-80
-90
-100
PWM = 19 kHz, PCT =100%
0
10
20
30
40
50
60
Frquency (kHz)

Figure 7

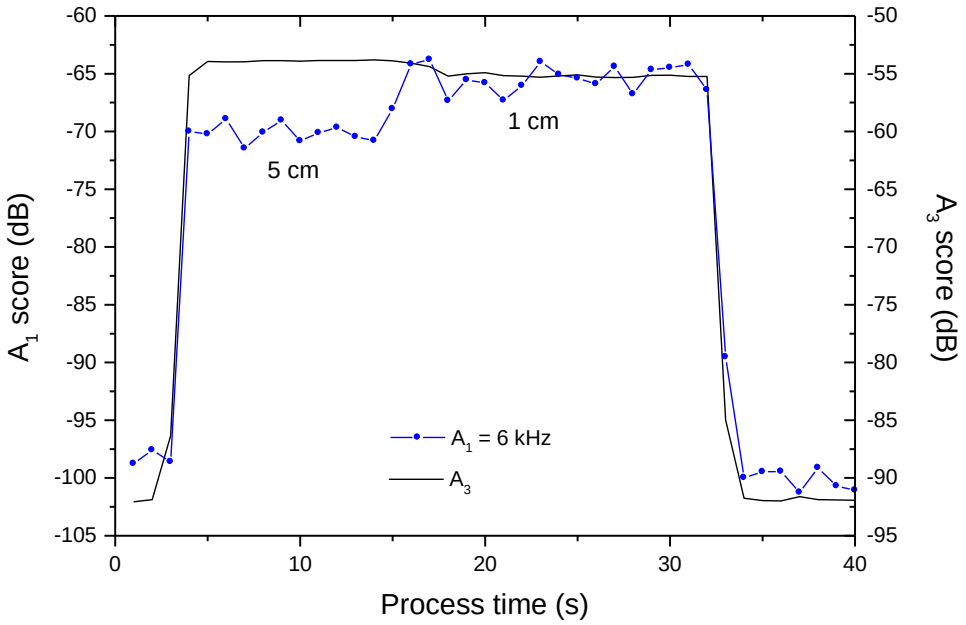
-60
-65
-70
-75
-80
-85
-90
-95
-100
-105
-50
-55
-60
-65
-70
-75
-80
-85
-90
-95
0
10
20
30
40
A1 score (dB)
A3 score (dB)
Process time (s)
5 cm
1 cm
A1 = 6 kHz
A3

Figure 8

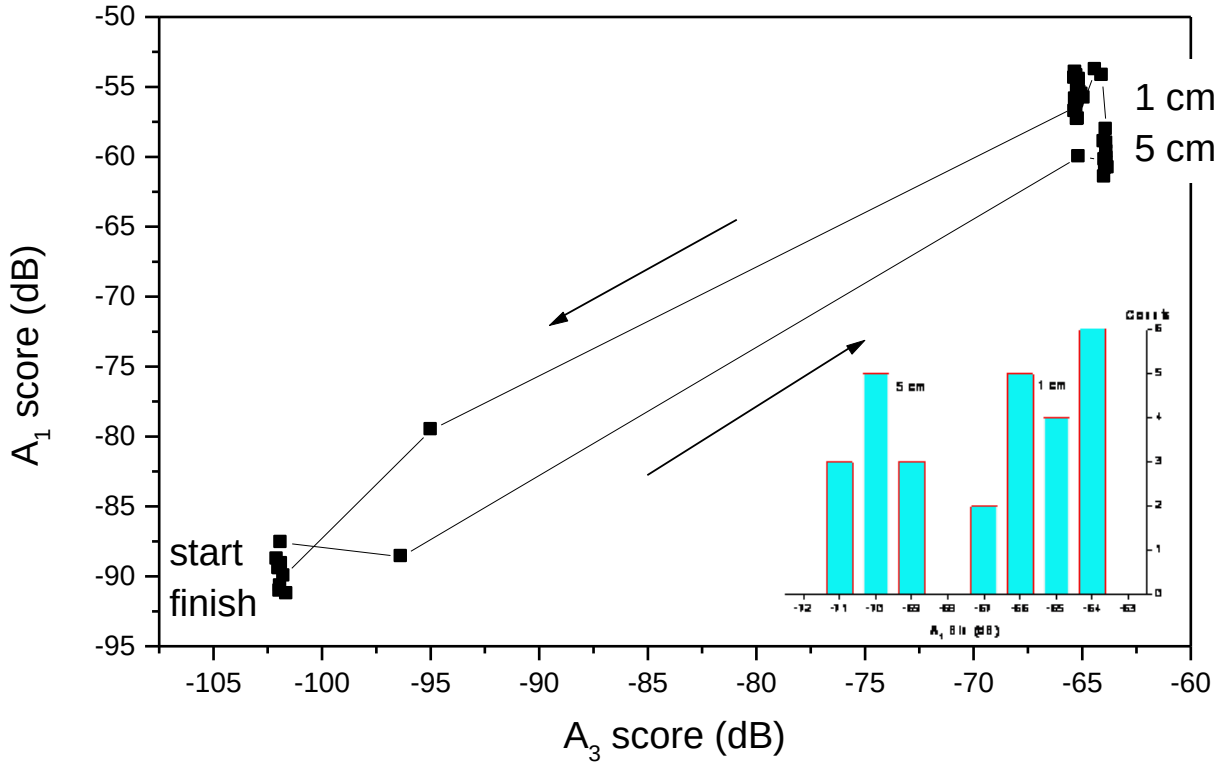
-50
-55
-60
-65
-70
-75
-80
-85
-90
-95
-105
-100
-95
-90
-85
-80
-75
-70
-65
-60
A1 score (dB)
A3 score (dB)
1 cm
5 cm
start
finish
5 cm
1 cm

Figure 9

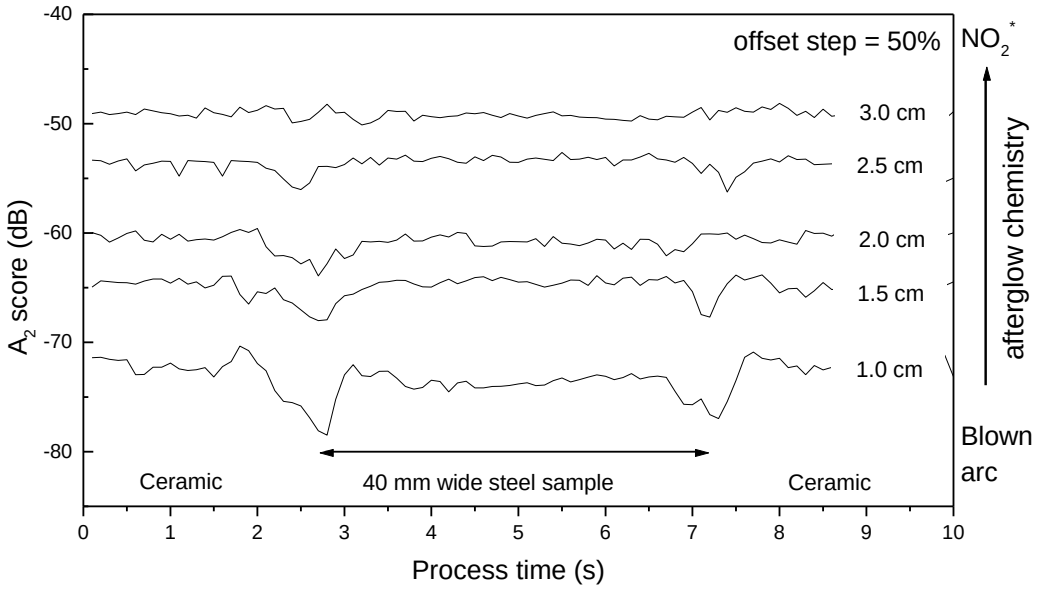
offset step = 50%
NO_2^*
3.0 cm
2.5 cm
2.0 cm
1.5 cm
1.0 cm
afterglow chemistry
Blown arc
Ceramic
40 mm wide steel sample
Ceramic
A_2 score (dB)
Process time (s)
-40
-50
-60
-70
-80
0
1
2
3
4
5
6
7
8
9
10

Figure 10

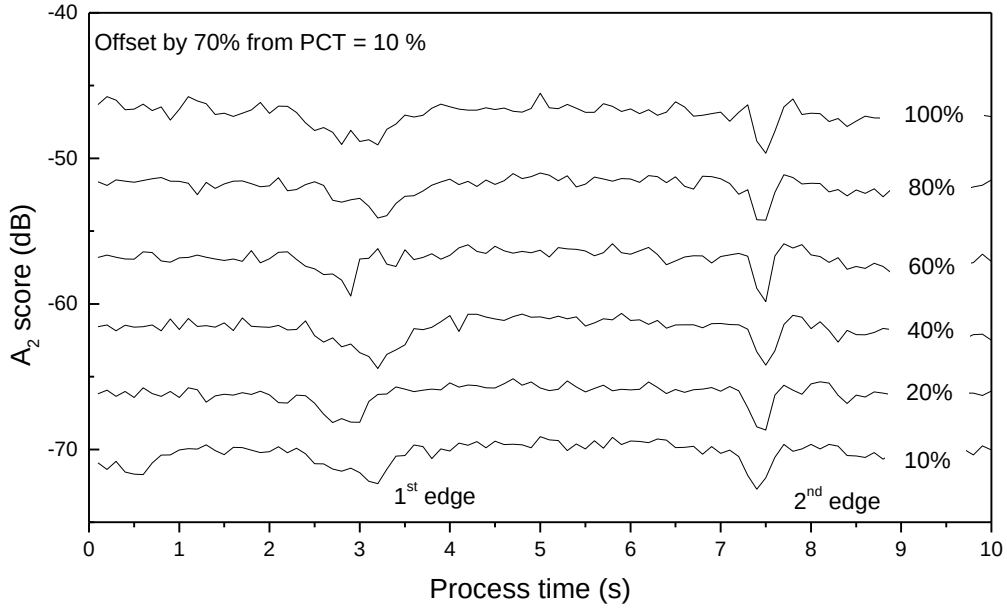
Offset by 70% from PCT = 10 %
100%
80%
60%
40%
20%
10%
1st edge
2nd edge
A2 score (dB)
Process time (s)
-40
-50
-60
-70
0
1
2
3
4
5
6
7
8
9
10

Figure 11

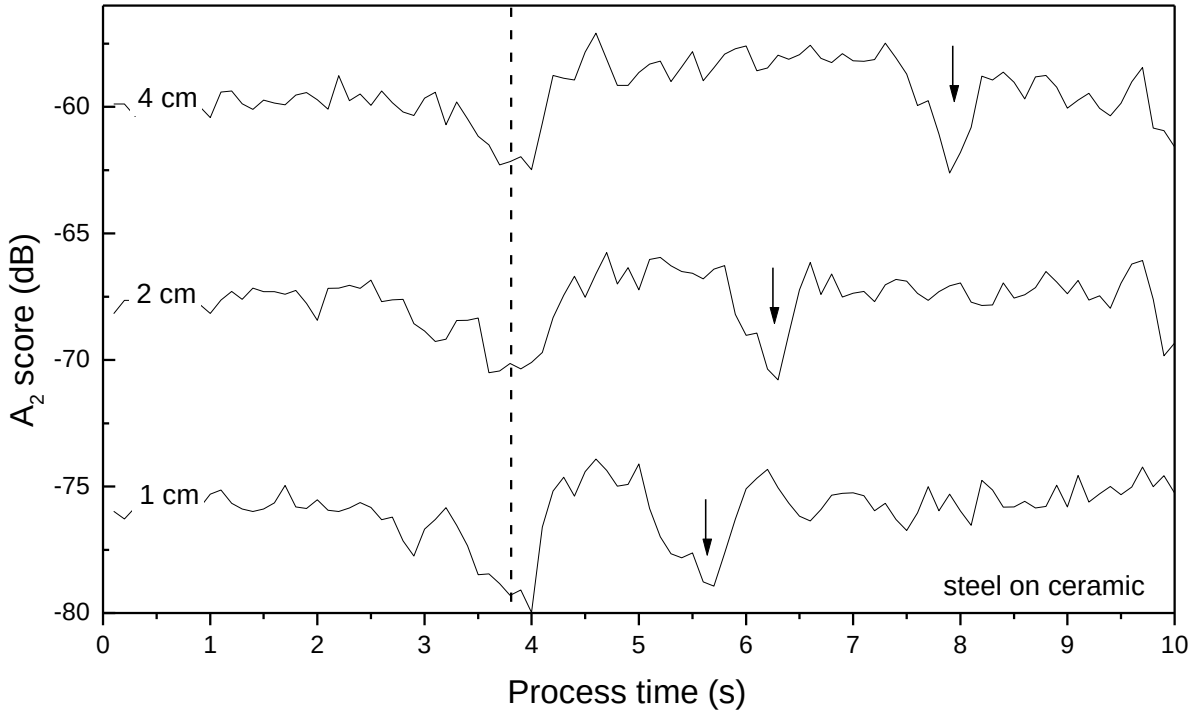
4 cm
2 cm
1 cm
steel on ceramic
A_2 score (dB)
-60
-65
-70
-75
-80
0
1
2
3
4
5
6
7
8
9
10
Process time (s)

Figure 12

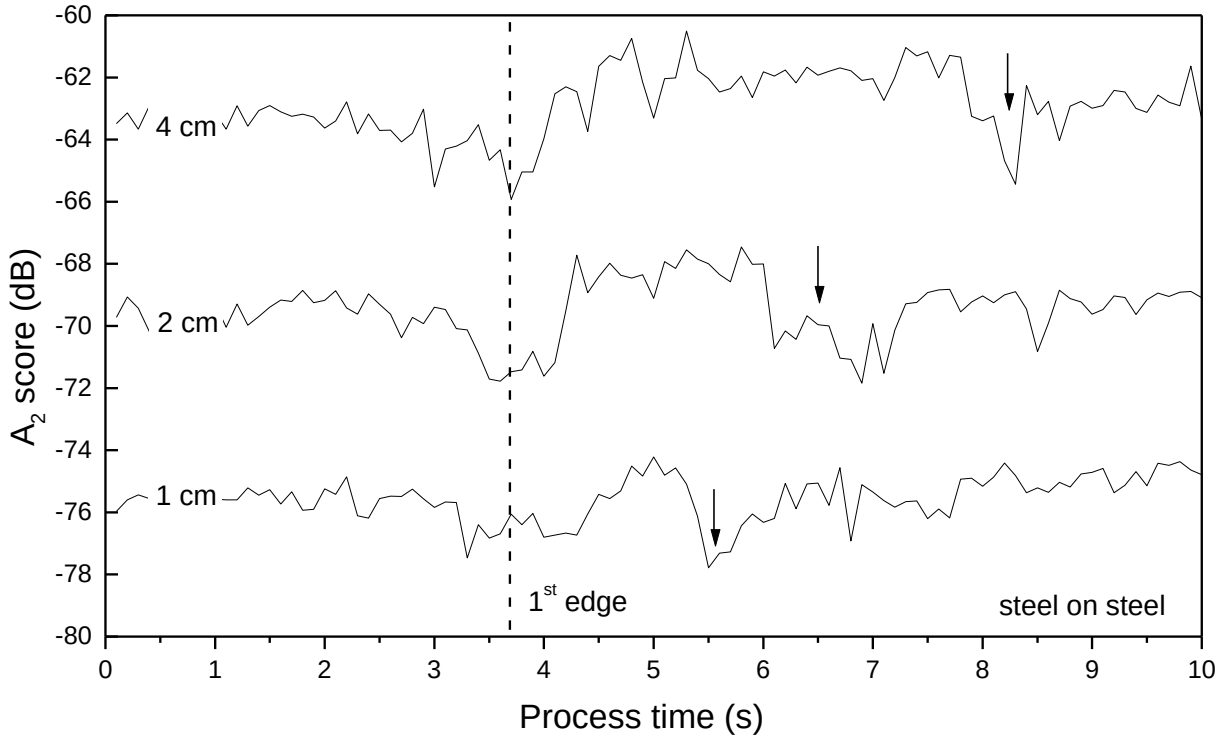
-60
-62
-64
-66
-68
-70
-72
-74
-76
-78
-80
A2 score (dB)
4 cm
2 cm
1 cm
1st edge
steel on steel
0
1
2
3
4
5
6
7
8
9
10
Process time (s)

Figure 13

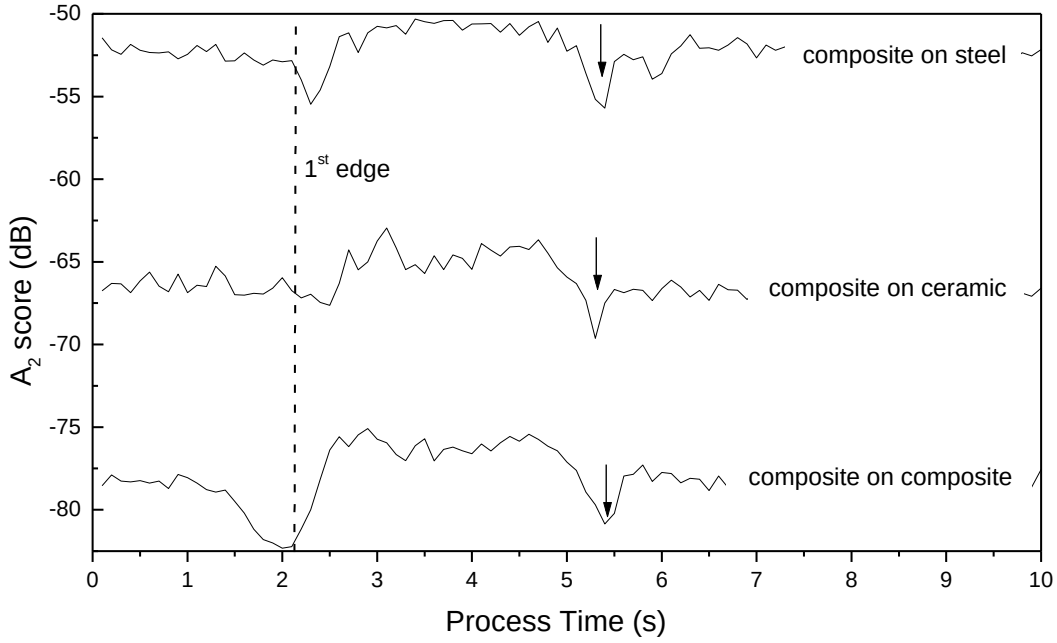
-50
-55
-60
-65
-70
-75
-80
A2 score (dB)
1st edge
composite on steel
composite on ceramic
composite on composite
0
1
2
3
4
5
6
7
8
9
10
Process Time (s)

Figure 14

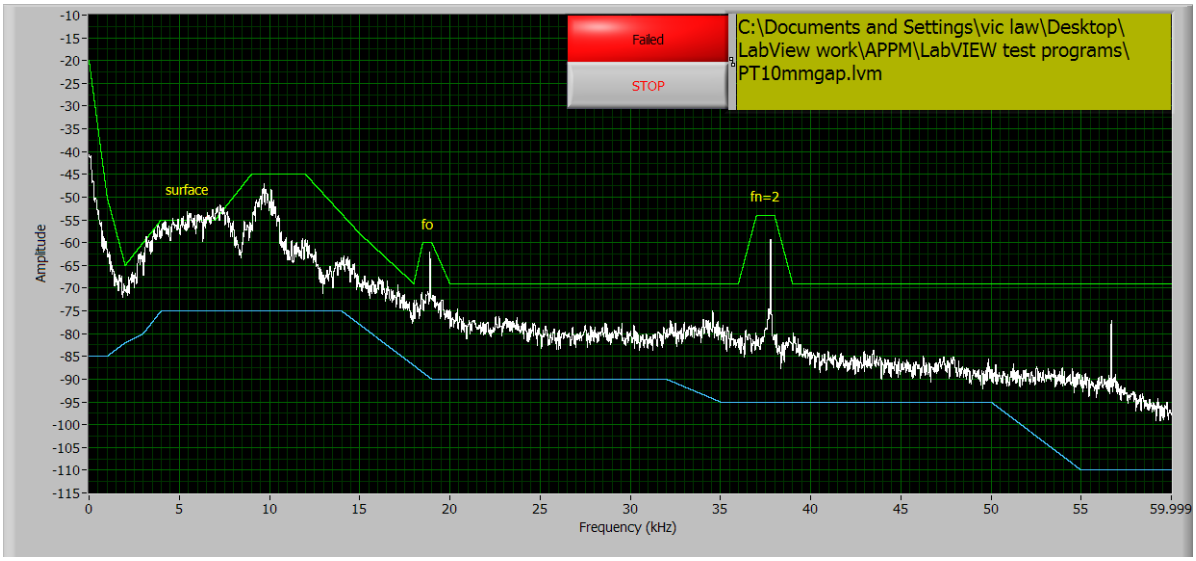
Failed
STOP
C:\Documents and Settings\vic law\Desktop\
LabView work\APPM\LabVIEW test programs\
PT10mmgap.lvm
surface
fo
fn=2
Amplitude
Frequency (kHz)
-10
-15
-20
-25
-30
-35
-40
-45
-50
-55
-60
-65
-70
-75
-80
-85
-90
-95
-100
-105
-110
-115
0
5
10
15
20
25
30
35
40
45
50
55
59.999